Available online at www.sciencedirect.com
SCIENCE DIRECT®
ELSEVIER
Journal of Marine Systems 44 (2004) 31–54
JOURNAL OF MARINE SYSTEMS
www.elsevier.com/locate/jmarsys

Influence of convection on mixed-layer evolution: comparison of two mixing parameterizations with buoys data in the Bay of Biscay

N. Jézéquel[a,*], A. Pichon[b], R. Mazé[a]

[a] Laboratoire de Physique des Océans, Université de Bretagne Occidentale, 29287 Brest Cedex, France
[b] Centre Militaire d'Océanographie, Etablissement Principal du Service Hydrographique et Océanographique de la Marine, 29603 Brest Cedex, France

Received 20 June 2001; accepted 10 March 2003

Abstract

In this study, we compare two 1-D mixing parameterizations developed by Gaspar et al. [J. Geophys. Res. C95 (C9) (1990) 16179] (G90) and Large et al. [Rev. Geophys. 32 (1994) 363] (L94), respectively. Both models are tested against drifting Marisonde bouys deployed in the Bay of Biscay during PRECOCE experiment (1997–1998) [Mariette, V., Ratsivalaka, C., Verbéque V., Leborgne, E., 1999. CAMPAGNE PREOCOCE (PREdiction du comportement des Couches superficielles de l'Océan le long des Côtes Européennes, Tomes 1, 2 and 3, Rapport EPSHOM/CMO/RE/NP 11 du 31 mai 1999]. Periods of stabilizing and destabilizing conditions are successively examined by using both realistic and schematic dynamical and thermodynamical air–sea fluxes. Schematic conditions applied over one diurnal cycle evidence the relative performance of G90 and L94 parameterizations as a function of surface inputs and stratification. The results obtained from these schematic cases are used to compare the results obtained by G90 and L94 over periods of 2 to 10 weeks along three Marisonde buoy trajectories. The ability of both models to simulate the seasonal thermocline formation in Spring as well as its destruction in Fall is discussed. If the nonlocal parameterization used by L94 is taken in its complete form (including the diapycnal mixing), it allows the mixed-layer deepening in Fall in a more satisfactory way than the local parameterization used by G90. The results obtained in Spring by both models are debatable.

Keywords: Buoy data; Surface mixed-layer; Mixing parameterizations; Eddy viscosity coefficients; Atmospheric forcing; Bay of Biscay

1. Introduction

Different parameterizations have been developed to model upper ocean mixing processes. From the bulk mixed-layer models up to the hierarchy of second-order moment closure schemes and to the recent nonlocal models, the choice of the parameterization used to simulate the mixing physics in the upper ocean depends, on the one hand, on the physical processes studied along with the climatological conditions observed and on the other hand, on both parameterizations precision and computational time.

Bulk models (Niiler and Kraus, 1977) attempt to represent the mixed-layer physics by integrating the

* Corresponding author. Tel.: +33-2-9889-2595.
E-mail address: nathalie.jezequel@wanadoo.fr (N. Jézéquel).

0924-7963/$ - see front matter © 2003 Published by Elsevier B.V.
doi:10.1016/j.jmarsys.2003.03.001

equations that governs momentum and scalar variables over the mixed-layer depth. These models assume that turbulence is efficient enough in the ocean upper layer to mix all physical properties inside this layer. The entrainment and detrainment of the mixed-layer are parameterized in term of momentum and buoyancy surface fluxes by using coefficients whose tuning depends on the different conditions met. Their advantage is their short computational time. Other models for simulating the upper ocean mixing are based on high-moment closure schemes for turbulent quantities; the most used of the second-order moment closure schemes is the level 2.5 developed by Mellor and Yamada (1982). A variant to them is the Turbulent Kinetic Energy TKE) model developed by Gaspar et al. (1990), denoted hereafter G90; it is interesting by its simple physics. Moreover, it adds only one TKE budget to the governing equations. In order to improve the major deficiency of previous schemes, that is the systematic underestimate of mixing across stabilizing density gradients, Large et al. (1994) developed the nonlocal model KPP (K-Profile Parameterization), denoted here L94; it parameterizes the different mixing processes that occur in the water column. It uses the similarity theory of turbulence in the near-surface layer contained into the boundary layer that is capable of penetrating the interior stratification. The depth of this boundary layer is defined as the depth at which turbulent structures injected at the sea-surface (induced by wind stress or by convection) can penetrate before becoming stable with respect to local buoyancy and velocity, i.e. stopped by stable density gradients. Below this boundary layer, the interior ocean is submitted to different mixing processes such as current shear instabilities, internal waves or double-diffusion.

In this paper, we will compare the two different mixing parameterizations developed in G90 and L94 to simulate the formation of the seasonal thermocline in Spring and its destruction in Fall under the climatological conditions found in the Bay of Biscay. This comparison will be based on in situ data measured along the trajectory of three Marisonde drifting buoys deployed over the cruise PRECOCE (Mariette et al., 1999). This cruise was conducted in the Bay of Biscay from September 1997 to June 1998 by the Etablissement Principal du Service Hydrographique et Océanographique de la Marine (EPSHOM, Brest, France) to observe the evolution of the ocean upper layer for three characteristic periods of the year: the destruction of the seasonal thermocline in Fall, the upper layer cooling in Winter and the formation of the seasonal thermocline in Spring. The Marisonde buoys were ship-deployed at three different times of the years 1997 and 1998 and provided us with temperature data measured at thermistors distributed between 0.5 and 200 m in depth with a sampling of 15 or 20 m. All in situ data were collected via Argos network. Marisonde buoys are interesting in 1-D studies because on the one hand, they follow the surface water mass over the 200-m surface layer and on the other hand they have not an important drag to the wind. Comparison between buoy data and 1-D mixing model results like those of Gaspar et al. (1990) and Large et al. (1994) has indeed to be made with caution for these models do not take into account the advective effects along the buoy trajectories. Another source of possible error in the comparison between in situ data and the mixing-model results comes from the momentum and buoyancy fluxes prescribed at the sea-surface. The fluxes used hereafter are those determined by the weather forecast model ARPEGE developed by METEO-FRANCE (Toulouse, France): they are available every 3 or 6 h all over the Bay of Biscay. Some discrepancies between the thermal budget given by the ARPEGE model and the heat content evolution of the water column obtained from in situ data have been observed in early Spring 1998 (Ratsivalaka, 1999).

Under these considerations, the comparison reported in this study will be developed in three sections. After a short review of the main theoretical aspects of models G90 and L94 in Section 2, we will, first, compare their results with in situ data along two buoy trajectories covering the stabilizing conditions characteristic of Spring in the Bay of Biscay (Section 3). This comparison will allow us to discuss the main differences between these two models over one diurnal Spring cycle, first, and then over longer periods of several weeks. We will next compare G90 and L94 results along one buoy trajectory, which covers the destabilizing conditions characteristic of Fall in the Bay of Biscay (Section 4). For each period, the effect of wind and night convection will be examined in details.

2. Theoretical aspects of the two models compared

The conservation of heat and momentum is written in the one-dimensional vertical case as:

$$\frac{\partial U}{\partial t} - fV = -\frac{\partial}{\partial z}\overline{(U' w')} \quad (1)$$

$$\frac{\partial V}{\partial t} + fU = -\frac{\partial}{\partial z}\overline{(V' w')} \quad (2)$$

$$\frac{\partial T}{\partial t} = \frac{F_{\mathrm{sol}}}{\rho_0 C_P}\frac{\partial I}{\partial z} - \frac{\partial}{\partial z}\overline{(T' w')} \quad (3)$$

U and V are the horizontal velocity components, T is temperature and w is the vertical velocity of water. The prime operator applied to each of these variables represents their turbulent fluctuations and the overbar denotes a time average. t is time and f is the Coriolis parameter. F_{sol} is the solar irradiance absorbed at the surface and $I(z)$ is the fraction of F_{sol} that penetrates to the depth z; ρ_0 and C_P are the reference density at the sea-surface and specific heat of sea water, respectively.

The surface turbulent fluxes are specified as follows:

$$-\rho_0 C_P\overline{(T' w')}_0 = F_{\mathrm{nsol}} = H + \mathrm{LE} + F_{\mathrm{ir}} \quad (4-\mathrm{a})$$

$$-\overline{(U' w')}_0 = \tau_x \quad (4-\mathrm{b})$$

$$-\overline{(V' w')}_0 = \tau_y \quad (4-\mathrm{c})$$

F_{nsol} is the "nonsolar" surface heat flux, the sum of the sensible (H), latent (LE) and net infrared (F_{ir}) heat fluxes, whereas $\vec{\tau} = (\tau_x, \tau_y)$ is the surface wind stress.

In most of closure schemes developed to solve Eqs. (1)–(3), the assumption is made that turbulent diffusion is down gradient, depending linearly on the local property gradient, with an appropriate eddy diffusivity K_x:

$$-\overline{w' X'} = K_x\frac{\partial X}{\partial z} \quad (5)$$

where X stands for momentum and scalar variables U, V, T and S.

We will compare here the two different parameterizations of turbulent diffusion that are shortly summarized hereafter.

2.1. TKE model developed by Gaspar et al. (1990) (G90)

The TKE model described here is based on the parameterization developed by Bougeault and Lacarére (1989) for atmospheric models and applied to oceanic simulations by G90. This parameterization consists in relating the diffusion coefficient K_x to the local TKE, e, of the water column together with the mixing length scale l_k determined from simple physical considerations and a calibration constant, c_k:

$$K_x = c_k l_k e^{\frac{1}{2}} \quad (6)$$

To close the system of Eqs. (1)–(3), the TKE budget equation for e has to be added under the following form:

$$\frac{\partial e}{\partial t} = -\frac{\partial}{\partial z}\left(\overline{e' w'} + \frac{\overline{p' w'}}{\rho_0}\right) - \overline{w' \vec{u'}}\left(\frac{\partial}{\partial z}\vec{U}\right) + \overline{b' w'} - \varphi \quad (7)$$

where p and φ stand for pressure and local dissipation, respectively. $b = g(\rho_0 - \rho)/\rho_0$ is the local buoyancy with ρ the density and ρ_0 the sea-surface one.

To close this equation, the concept of turbulent diffusion (Eq. (5)) is used to parameterize the vertical flux of TKE in Eq. (7) as a function of turbulent local gradient of TKE, e, and of the turbulent diffusion coefficient, K_e, given by (Eq. (6)):

$$-\left(\overline{e' w'} + \frac{\overline{p' w'}}{\rho_0}\right) = K_e\frac{\partial e}{\partial z} \text{ with } K_e = K_x \quad (8)$$

The dissipation term in Eq. (7) is parameterized using the Kolmogorov theory (1942):

$$\varphi = \frac{c_\varphi e^{\frac{3}{2}}}{l_\varphi} \quad (9)$$

where c_φ is a calibration constant, and l_φ is a characteristic length of dissipation.

The complete set of Eqs. (1)–(3) and (7) to be solved, rewritten using Eqs. (6), (8) and (9), is found in Appendix A. In order to completely solve these equations, l_φ, l_k as well as calibration constants c_φ and c_k have to be determinated.

One of the assets of the parameterization developed in G90 is the use of two different lengths, l_φ and l_k, for dissipation and mixing, respectively:

$$l_\varphi = (l_U l_D)^{\frac{1}{2}} \qquad (10-\mathrm{a})$$

$$l_k = min(l_U, l_D) \qquad (10-\mathrm{b})$$

where at any depth z, l_U and l_D are the distances traveled upward and downward by a particle converting all of its original TKE into potential energy. These two lengths are given by the balance between TKE and potential energy along this travel:

$$\frac{g}{\rho_0}\int_z^{(z+l_U)}(\rho(z)-\rho(z'))\mathrm{d}z' = e(z) \qquad (11-\mathrm{a})$$

$$\frac{g}{\rho_0}\int_z^{(z-l_D)}(\rho(z)-\rho(z'))\mathrm{d}z' = e(z) \qquad (11-\mathrm{b})$$

The two constants c_k and c_φ have been calibrated from laboratory and atmospheric results: Bougeault and Lacarrére (1989) showed that the value $c_\varphi = 0.7$ was adequate. The choice of a value for c is based on the determination of a mixing efficiency coefficient deduced from oceanic observations. Gaspar et al. (1990) found it to be $c_k = 0.1$.

A minimum value $\bar{e}_{\min} = 10^{-6}$ s^{-2} is specified for TKE in order to obtain diffusion rates in the thermocline.

2.2. KPP nonlocal model developed by Large et al. (1994) (L94)

The KPP nonlocal model developed in L94 allowed them to take into account the two distinct regimes found in the ocean: (i) the mixing observed in the surface boundary layer, due to stabilizing, destabilizing or wind-driven surface forcing and (ii) the mixing in the ocean interior due to three main mechanisms, i.e. background internal waves, current shear instabilities and double-diffusion. This model is aimed at determining the coefficient of turbulent diffusion corresponding to these different regimes. To do this, the surface boundary layer (BL), of depth h, is split into two distinct zones (Fig. 1): the first zone, the near-surface layer of depth with ε = 0.1, is submitted to the similarity theory of turbulence (Large et al., 1994). The second one makes the transition between the near-surface layer and the ocean interior.

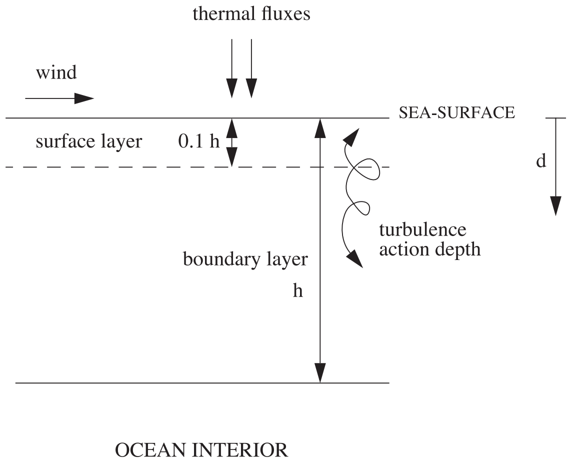

Fig. 1. Description of the different mixing areas used by Large et al. (1994).

2.2.1. Surface boundary layer h

The diffusivity profile in the surface boundary layer is expressed as the product of a turbulent velocity scale w_x by the BL depth h and G, a dimensionless form function, as follows:

$$K_x(\sigma) = hw_x(\sigma)G(\sigma) \qquad (12)$$

where σ=(d/h), with d the distance from the sea-surface. Index x stands for scalar variables, i.e. salinity S and temperature T as well as for dynamical ones, i.e. velocity components U and V. Functions $w_x(\sigma)$ and $G(\sigma)$ are defined in Appendix B. All these assumptions are issued from L94.

The important parameter to be determined in L94 is the extension h of the oceanic boundary layer: it is dependent on the atmospheric forcing at the sea-surface as well as on the local buoyancy and velocity profiles in the water column, $B(d)$ and $V(d)$, respectively. A Richardson number related to the surface is defined as:

$$Ri_b(d) = \frac{(B_r - B(d))d}{|V_r - V(d)|^2 + V_t^2(d)} \qquad (13)$$

B_r and V_r are the mean buoyancy and velocity over the near-surface layer $0<d<\varepsilon h$. The depth h is stated equal to the smallest value of d for which $Ri_b(d)$ is equal to a critical value Ri_c (=0.3 in our simulations). The physical meaning of this definition is that the turbulent structures present in the near-surface layer of mean velocity V_r and buoyancy B_r must be able to penetrate to a depth h where they become stable with respect to the local buoyancy and velocity.

The destabilizing term $V_t^2(d)$ at the denominator of relation (13) acts under pure convection or little mean shear conditions. It takes the following form:

$$V_t^2 = \frac{C_V(-\beta_T)^{\frac{1}{2}}}{R_{ic}\kappa^2}(C_S\varepsilon)^{-\frac{1}{2}}\mathrm{d}Nw_x \tag{14}$$

where C_V, C_S, β_T are parameters specified in L94, $\kappa=0.4$ is von Karman's constant N^2 is the local Brunt–Vaisala frequency.

2.2.2. Ocean interior

In L94, the interior mixing is parameterized as the superposition of two terms:

$$K_x(d) = K_x^{\mathrm{S}}(d) + K_x^{\mathrm{W}}(d) \tag{15}$$

• The first one denotes the mixing due to a shear instability characterized by the following local Richardson number:

$$Ri_g = \frac{N^2}{\left(\frac{\partial U}{\partial z}\right)^2 + \left(\frac{\partial V}{\partial z}\right)^2}$$

The corresponding diffusivity is parameterized as a function of Ri_g as follows:

$$\frac{K_x^{\mathrm{S}}}{K^0} = 1 \quad Ri_g < 0 \tag{16 – a}$$

$$\frac{K_x^{\mathrm{S}}}{K^0} = \left(1 - \left(\frac{Ri_g}{Ri_0}\right)^2\right)^{p_1} \quad 0 < Ri_g < Ri_0 \tag{16 – b}$$

$$\frac{K_x^{\mathrm{S}}}{K^0} = 0 \quad Ri_0 < Ri_g \tag{16 – c}$$

where $K^0 = 50\times10^{-4}$ m^2; $Ri_0 = 0.7$ and $p_1 = 3$.

• The second one is due to the internal waves breaking in the ocean interior. The corresponding diffusivity coefficients take the following form for momentum (m) and scalar (s) variables:

$$K_{\mathrm{m}}^{w} = 1.0\times10^{-4}\ \mathrm{m^2/s}\ \text{and}$$
$$K_{\mathrm{s}}^{\mathrm{w}} = 0.1\times10^{-4}\ \mathrm{m^2/s}$$

A third term related to the double-diffusion effect can be added in Eq. (15).

2.3. Aim of the simulations

Besides the parameterization used for the turbulent diffusion coefficient (Eq. (6) for G90 and Eq. (12) for L94), these two models differ in two main points which are the following ones:

(i) the interior mixing (Eqs. (16-a,b,c)) used in L94 which is not taken into account in G90 except by the mean of the minimum value $\bar{e}_{\mathrm{min}}$ for TKE;
(ii) the nonlocal destabilizing term V_t^2 (Eq. (14)) acting in situations of pure convection or weak wind in L94 and which has no equivalent in G90.

One objective of this study is to determine the relative importance of these two terms in simulating the evolution of the upper 200-m surface layer in two types of conditions: (1) Spring conditions of strong warming of the upper layer and (2) Fall conditions of thermocline destruction with strong wind events. In particular, we will examine the relative part of wind events and convection in these different simulations. To do this, we will compare the G90 version presented in Section 2.2 with the complete L94 version presented in Section 2.3 as well as with this version without diapycnal mixing (Eqs. (16-a,b,c)) nor destabilizing term (Eq. (14)).

3. Cases of stabilizing-dominant conditions

Preliminary studies were achieved to define the numerical and physical parameters used by G90 and L94 models. It was found that the Jerlovi's parameter has a stronger influence on the results than the vertical discretization. The solar exponential penetration has been adjusted according to the measurements made in the Bay of Biscay during the PRECOCE experiment: in Spring the water is found of type 3. Furthermore, a study concerning the stability of the two models led us to choose a time step $dt = 600$ s and a spatial vertical step $dz = 5$ m for the simulations. Salinity will be assumed equal to 35 psu and constant.

We will, first, compare G90 and L94 results with in situ data recorded in Spring along two buoy trajectories; they cover the formation of the seasonal thermocline. The first in situ data set along Marisonde buoy 15534 is characterized by a balanced thermal budget for a weakly stratified water column, i.e. the conditions found in early Spring; the second data set along Marisonde buoy 15506 corresponds to the conditions found at the end of Spring, i.e. a globally positive thermal budget for a seasonal thermocline in formation. For each buoy, we will examine global simulations run with ARPEGE realistic fluxes at the sea-surface. Then, we will define schematic fluxes to discuss the relative behaviour of G90 and L94 parameterizations over the diurnal cycle.

3.1. Global simulations

3.1.1. Balanced thermal budget for a weakly stratified water column

Buoy 15534 was deployed on March 27, 1998 at position (46°08N–14°30W) to be recovered on June 12, 1998 at position (45°08N–10°28W). Its trajectory was centered in the middle of the Bay of Biscay. The period of interest here extends from May 1 to June 6, 1998. The thermal fluxes and wind stresses forcing G90 and L94 models at the sea-surface are issued from the weather forecast model ARPEGE and extracted along the buoy trajectory (Fig. 2a and b): these fluxes range within 250 and 550 W/m^2 on day and between -200 and -50 W/m^2 at night. The corresponding wind intensities vary from 2 to 11 m/s. The ocean temperature evolution at nine different depths along the buoy trajectory is shown in Fig. 2c, which exhibits a weak M_2 internal tide variation in temperature evolution. Internal tide oscillations can be particularly strong in the Bay of Biscay. In Fall, when these internal tides are the strongest, they can be responsible for significant mixing resulting in cool water patches observed at the shelf break. In this data–model comparison, we chose buoys whose trajectory is far enough from the shelf break. Moreover, internal tides are weakest in Spring, and consequently also the mixing they induce. So, the internal tides mixing influence has not to be taken into account in the following 1-D simulations.

The relative behaviour of G90 and L94 along buoy 15534 trajectory is compared in Fig. 3 and allows us to extract two main distinct periods directly related to the wind intensity (Fig. 2b):

- Period 1 between days 5 and 15 is characterized by a low wind intensity of 5 m/s. Over this period, G90 and L94 behaviours are similar: at day 15 both models predict a temperature of 14.5 °C at the 2.5-m depth and of 13.8 °C at 15 m.
- Period 2 extends from day 15 to day 25: the wind is stronger than over period 1 with a mean intensity of 8 m/s. From day 15, G90 and L94 start to behave in a different way: according to L94, the mixed-layer reaches the 15-m depth at day 20. G90 predicts that only at day 25. Between days 20 and 25, level 30 m undergoes a strong warming of half a degree with L94, whereas G90 shows a corresponding increase of only 0.1 °C at the same level.

The cross-examination of in situ data with model results allows us to distinguish in the data–models comparison the same two periods as previously. Up to day 15, as long as the wind is weak (period 1), G90 and L94 similar results are in good accordance with in situ data. In that case, advective effects can be neglected and the 1-D assumption is applicable. From day 15, when the wind becomes stronger (period 2), we observe an excessive warming of the near-surface upper layer obtained by G90, whereas L94 tends to underestimate this warming by a stronger mixing in the 15-m upper layer. Furthermore, at days 28 and 33, the 30-m temperature observed in in situ data shows two warming events that are not correlated with sea-surface fluxes. They are not observed in TG90 and L94 simulations. Over period 2, advective effects can then not be neglected and conclusions have to be made with caution. Fig. 3b compares the results obtained with L94 without diapycnal mixing (Eqs. (16-a,b,c)). The lack of diapycnal mixing leads to delay the mixing of the 15-m upper layer from day 20 to day 30. This also leads to the increase of the sea-surface temperature (SST) of one Celsius degree in period 2. Tests not compiled here

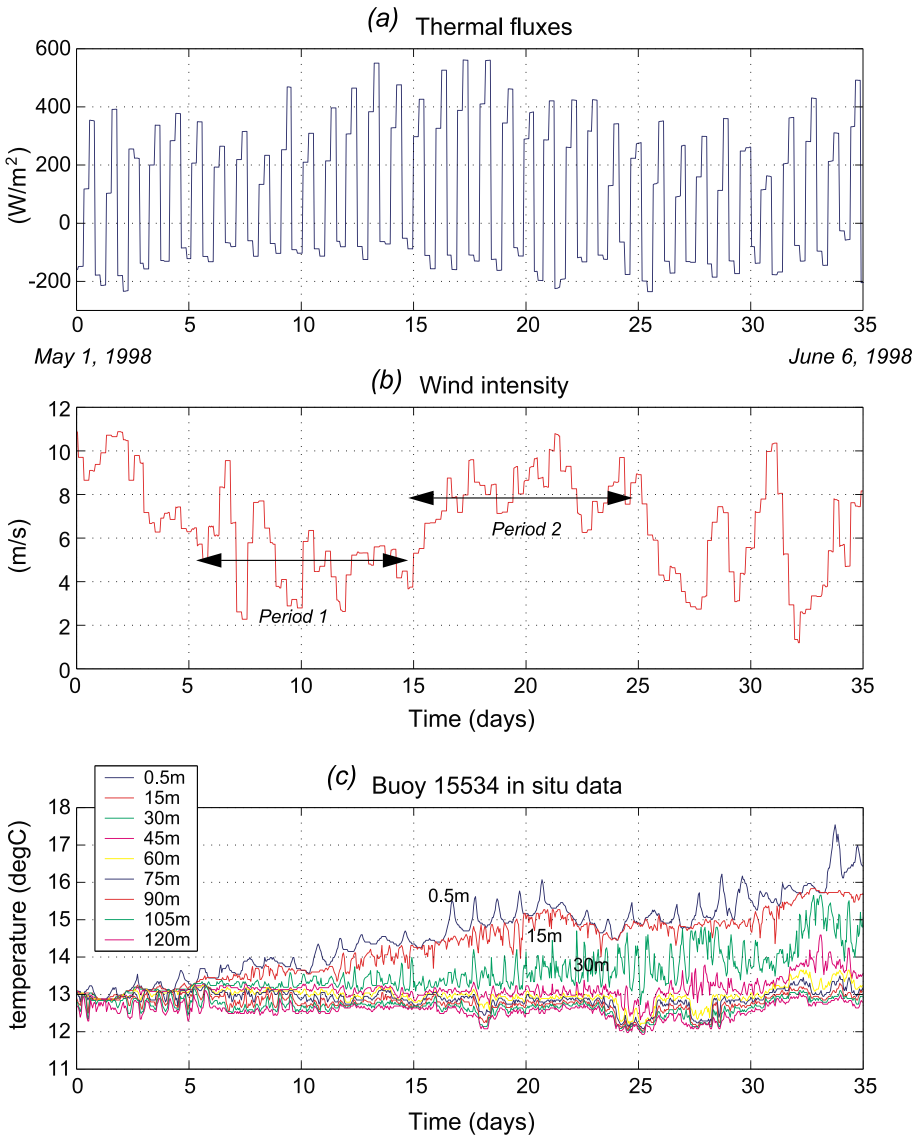

Fig. 2. Thermal fluxes (a) and wind intensity (b) issued from the weather forecast model ARPEGE (METEO-FRANCE, Toulouse) along buoy 15534 trajectory between May 1 and June 6, 1998. (c) Raw temperature evolution at thermistor depths 0.5, 15, 30, 45, 60, 75, 90, 105 and 120 m along the buoy 15534 trajectory.

showed that the influence of destabilizing term (Eq. (14)) is minor in these conditions of weak convection.

3.1.2. Positive thermal budget for a seasonal thermocline in formation

Let us now examine the behaviour of both models under stronger diurnal solar fluxes with or without significant wind intensity. These conditions are those observed in late Spring; they lead to a strong diurnal warming of the upper surface layer.

Buoy 15506 was deployed on June 3, 1998 at position (45°42N–07°05W) to be recovered on July 18, 1998 at position (45°41N–04°26W). The period of interest, here, extends from June 14 to 26, 1998. The buoy trajectory is also centered in the middle of the Bay of Biscay. In order to improve the data–

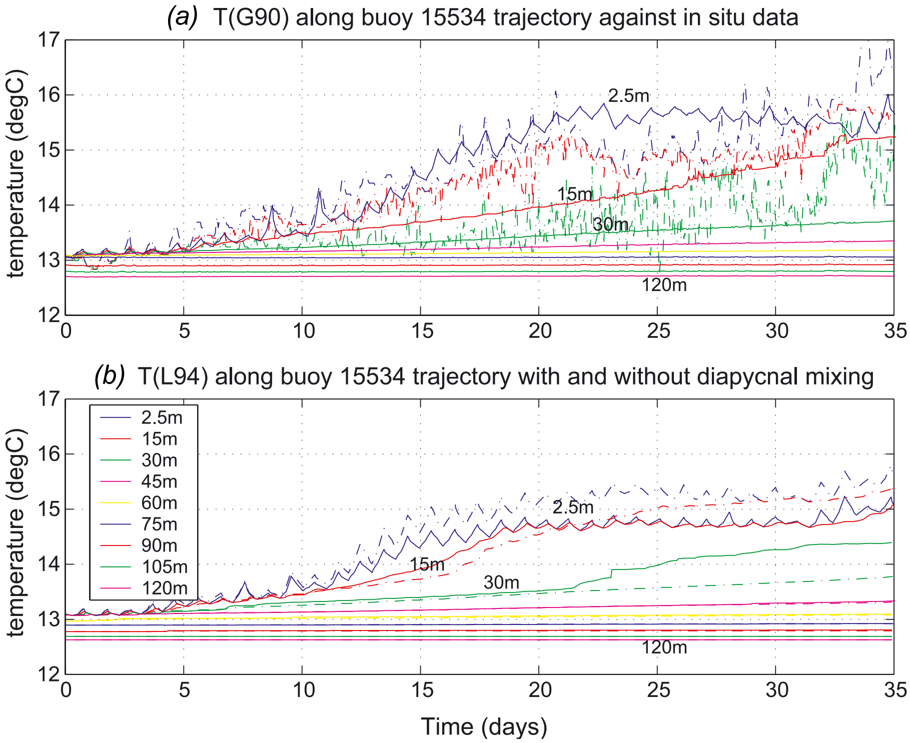

Fig. 3. (a) Temperature evolution at depths 2.5, 15, 30, 45, 60, 75, 90, 105 and 120 m simulated by model G90 (full line) in comparison with in situ data (dashed line); (b) L94 corresponding simulation with (full line) and without (dashed line) diapycnal mixing (Eqs. (16-a,b,c)).

models comparison, we used more Saccurate infrared fluxes than those predicted by ARPEGE during Spring 1998: these fluxes are issued from the cloud cover data given by satellite METEOSAT. They are only available for the period June 14 to 30 (Ratsivalaka, 1999). The fluxes extracted along the buoy trajectory show a clearly positive thermal budget of 750 W/m^2 on day and of -100 W/m^2 at night associated with periods of moderate and low wind (Fig. 4a and b). We can define here three periods corresponding to wind intensities: period 0 (from day 1 to 5) and period 2 (from days 7 to 10) are characterized by a wind intensity lower than 5 m/s, whereas period 1 (from days 7 to 10) is characterized by a 10-m/s wind. Fig. 4c displays the raw data along the buoy trajectory. The influence of wind intensity is obvious over periods 1 and 2: under moderate wind conditions (period 1), the sea-surface temperature (SST) is stable, whereas under low wind conditions (period 2) it rises by 2 °C on day 9.

Fig. 5a and b depicts the G90 and L94 simulation results along the buoy trajectory. One can note in these results the three different regimes corresponding to wind intensities. Over periods 0 and 2, there is a high difference in G90 and L94 predictions about the sea-surface warming. In particular, at level 2.5 m and noon on day 9 G90 gives a SST 4 °C higher than L94. On period 1 of higher wind, both models predict a stable SST. Fig. 5b compares L94 results obtained with and without diapycnal mixing (Eqs. (16-a,b,c)). As in Section 3.1.1, the influence of destabilizing term (Eq. (14)) is minor and is not presented here. The diapycnal mixing is particularly active in stronger wind events, i.e. over period 1. Its influence is negligible over periods 0 and 2. Whereas the in situ SST obtained along the buoy trajectory is closest to L94 results in period 1, it stands between G90 and L94 results in period 2. However, the lack of in situ data between the sea-surface and the 20-m depth does not allow us to improve this comparison in term of mixing of the upper layer.

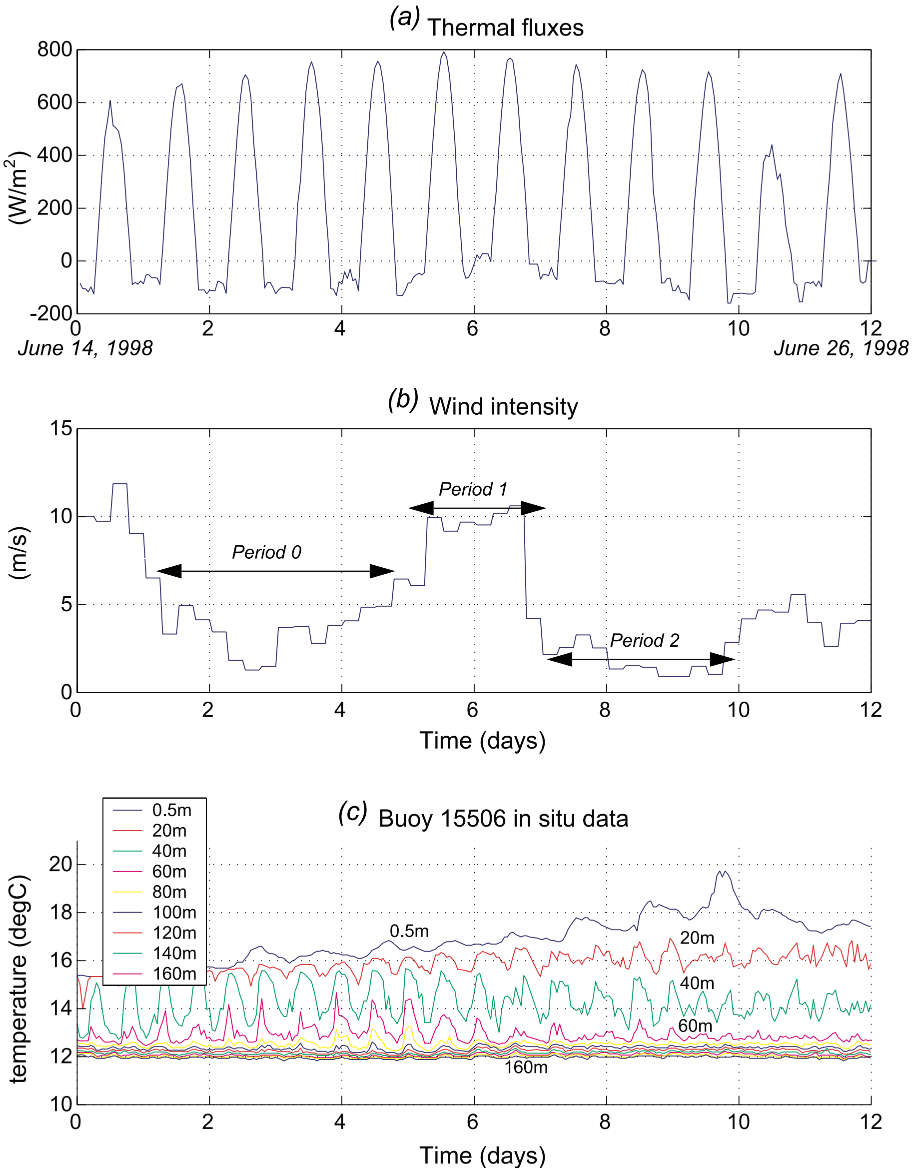

Fig. 4. Thermal fluxes (a) and wind intensity (b) along buoy 15506 trajectory between June 14 and 26, 1998. (c) Raw temperature evolution at thermistor depths 0.5, 20, 40, 60, 80, 100, 120, 140 and 160 m along the buoy 15534 trajectory.

3.2. Schematic diurnal tests

To compare the relative behaviour of G90 and L94 under these conditions of Spring warming, let us use periodical diurnal thermal fluxes representative of the mean conditions corresponding to realistic fluxes and wind observed along buoy 15534 trajectory (Fig. 2). The sinusoidal diurnal flux of 300 W/m^2 and the constant nocturnal flux of -100 W/m^2 presented in Fig. 6b are introduced as sea-surface forcing for both models. These models are initialized with the quasi-homogeneous temperature profile found in in situ 15534 data at day 5 (Fig. 6a).

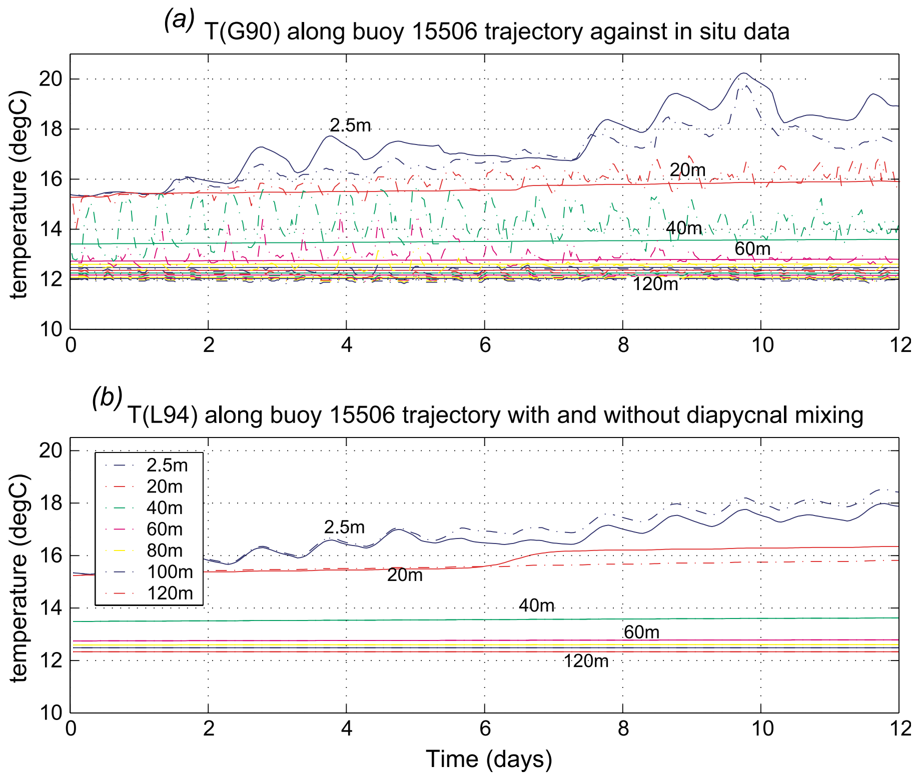

Fig. 5. (a) Temperature evolution at depths 2.5, 20, 40, 60, 80, 100, 120, 140 and 160 m simulated by model G90 (full line) in comparison with in situ data (dashed line); (b) L94 corresponding simulation with (full line) and without (dashed line) diapycnal mixing (Eqs. (16-a,b,c)).

We will focus on the effect of wind (no wind or a 5-m/s constant wind). Each simulation uses the periodical thermal fluxes shown in Fig. 6 over one diurnal cycle. G90 results are compared with those obtained with L94 in its complete form in Fig. 7a and b without wind and in Fig. 7c and d with the 5-m/s constant wind. The 5-m/s wind results obtained by using L94 without diapycnal mixing (Eqs. (16-a,b,c)) are shown in Fig. 7e, whereas the same results obtained without diapycnal mixing nor destabilizing term (Eq. (14)) are shown in Fig. 7f.

Without wind (Fig. 7a and b), G90 and L94 give alike results over the first 12 h of positive thermal fluxes. When night convection starts (hour 13) and up to hour 24, G90 and L94 act in a different way: levels 2.5 and 7.5 m are progressively mixed in L94 from the first hours of night convection till hour 21 when these two levels reach the same temperature. G90 does not induce such a mixing during night convection.

With a 5-m/s wind (Fig. 7c and d) now, the two models do not react in the same way under the stabilizing conditions of the first 12 h. Over this stabilizing period, there is much more mixing in G90 temperature results than in L94 ones: at hour 12, the temperature difference between levels 2.5 and 7.5 m is cut by two with G90 compared to L94. From hour 13 when night convection starts, the situation is totally different. The action of mixing goes deeper in the water column in L94 results: it reaches level 17.5 m at hour 22. On the other hand, G90-evaluated mixing does not allow the homogenization of the upper layer and creates inversions in the temperature profile due to the local character of the parameterization.

Let us now examine the results obtained using L94 without diapycnal mixing (Eqs. (16-a,b,c)) nor destabilizing term (Eq. (14)). Without wind, results obtained without these terms are nearly the same as in Fig. 7b, so they are not shown here: the mixing

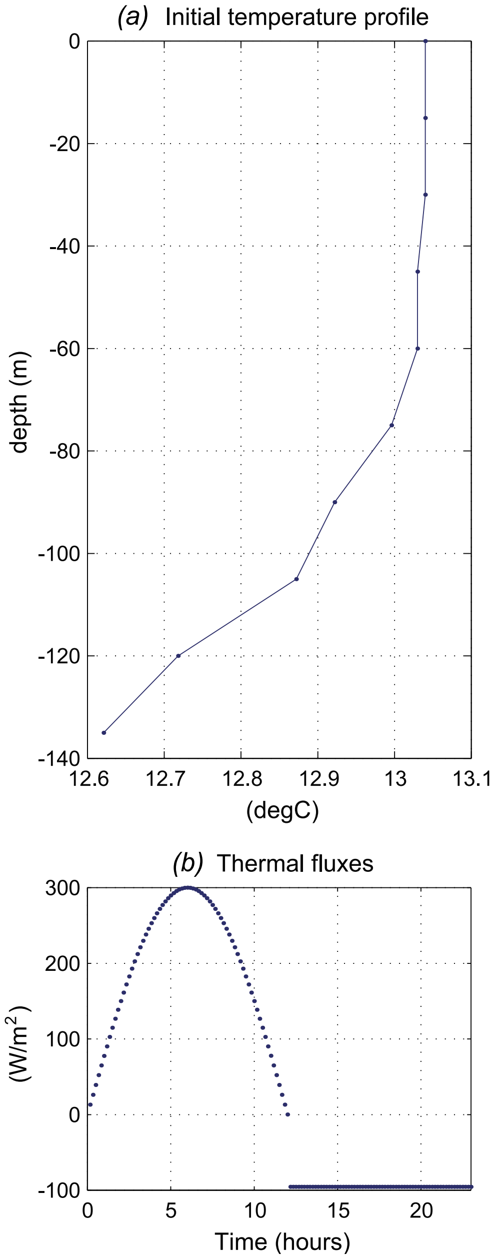

Fig. 6. Initial temperature profile (a) and periodical thermal fluxes (b) used for schematic diurnal tests in the air–sea fluxes conditions found along buoy 15534 trajectory.

observed during night convection between levels 7.5 and 12.5 m in Fig. 7b is therefore not attributable to any of these two terms but to the non-local determination (Eq. (13)) of the BL depth h used by L94. With a 5-m/s constant wind now, the influence of diapycnal mixing is dominating in L94 results, as shown by comparing Fig. 7d and e. Without this term, the SST increase during day is nearly the same as without wind. If we now compare L94 results without diapycnal mixing nor destabilizing term (Eq. (14)) (Fig. 7f) with G90 results presented in Fig. 7c, we can see that during day, the SST increase is more important by L94 than by G90, whereas during night G90 parameterization induces temperature inversions in the 12.5-m upper layer.

G90- and L94-parameterizations give, then, radically different results in the stabilizing and destabilizing conditions observed here. As shown in Fig. 8a to d for the diffusivity coefficients corresponding to G90 and L94 simulations shown in Fig. 7a to d (L94 with diapycnal mixing (Eqs. (16-a,b,c)) and destabilizing term (Eq. (14))), whereas G90 tends to determine mixing coefficients of similar amplitude for a given wind under stabilizing or destabilizing conditions (Fig. 8c), L94 radically distinguishes these two types of conditions (Fig. 8d). To understand these differences, let us come back succinctly to the vertical mixing parameterizations respectively used by G90 and L94. G90 local parameterization (Eq. (6)) is based on the evaluation of the local TKE in the water column (Eq. (7)) as a function of both the local velocity shear, local buoyancy and the TKE injected at the sea-surface by wind (u*). The mixing length l_k is determined by converting the TKE available at each depth into potential energy. For a same wind intensity, the TKE evaluated in stabilizing as in destabilizing conditions is nearly the same and leads to an equivalent mixing coefficient amplitude. On the other hand, L94 nonlocal parameterization (Eq. (12)) uses the vertical turbulent velocity w_x. This latter is proportional to ku* and inversely proportional to the dimensionless profiles issued from the similarity theory applied to the near-surface layer (Appendix B, Eq. (B-2-a) and (B-2-b). As shown in Fig. 2 in Large et al. (1994) the turbulent velocity w_x has not the same behaviour in stabilizing and destabilizing conditions. This explains the differences observed between night and day for the L94 results. By applying the same conditions for thermal fluxes without wind (or with a weak wind) over a few days, G90 leads then to a strong increase of the SST (Fig. 7a) for it is unable to induce enough mixing during night convection. On

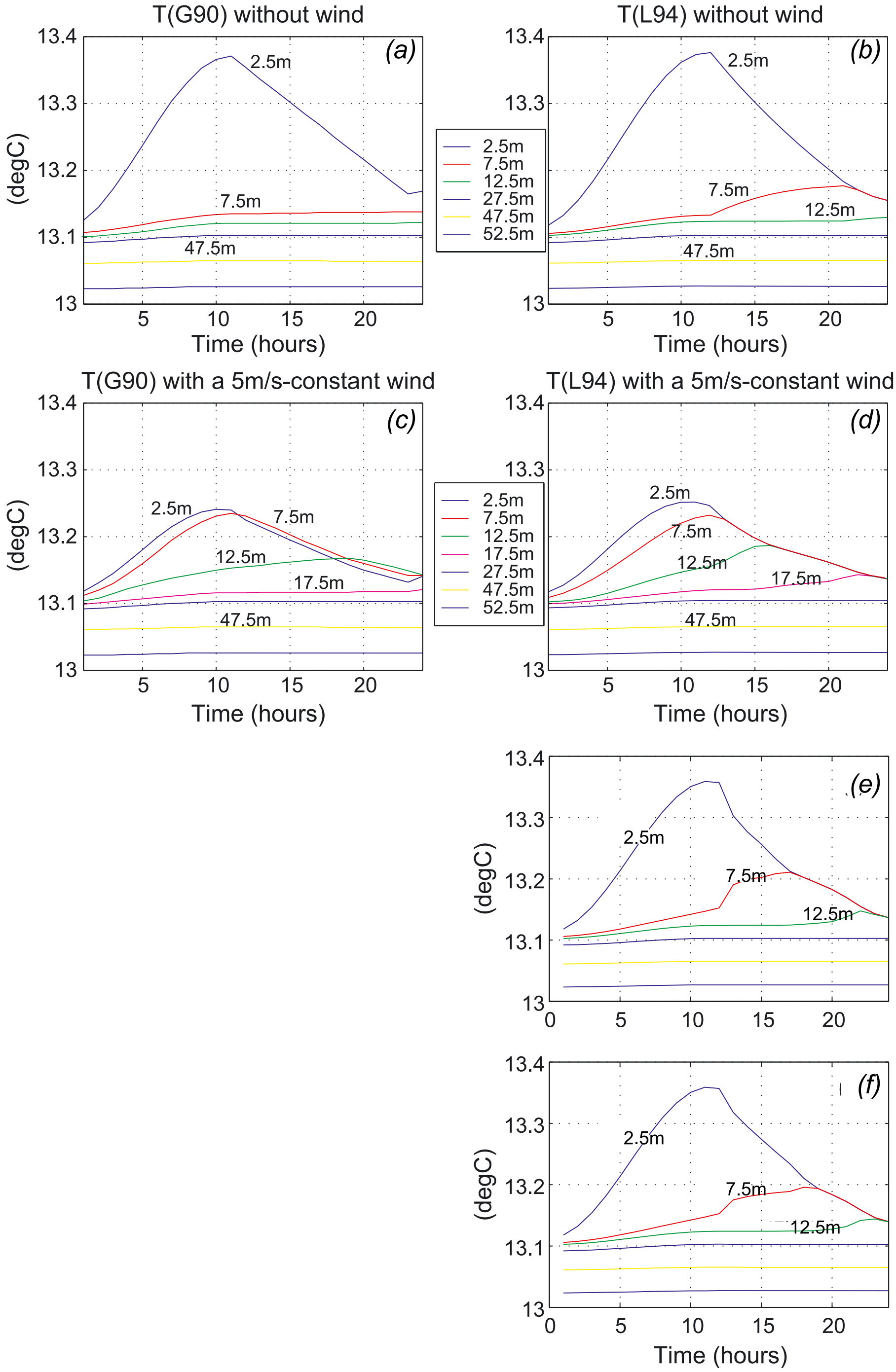

Fig. 7. Comparison of temperature evolution at six different depths over one diurnal cycle using thermal fluxes shown in Fig. 6, initialized with the stratification denoted Case 1 and obtained with: (a) G90 without wind, (b) L94 without wind, (c) G90 with a 5 m/s wind, (d) L94 with a 5-m/s wind, (e) L94 with a 5-m/s wind and without diapycnal mixing (Eqs. (16-a,b,c)) and (f) L94 with a 5-m/s wind and without diapycnal mixing (Eqs. (16-a,b,c)) nor destabilizing term (Eq. (14)).

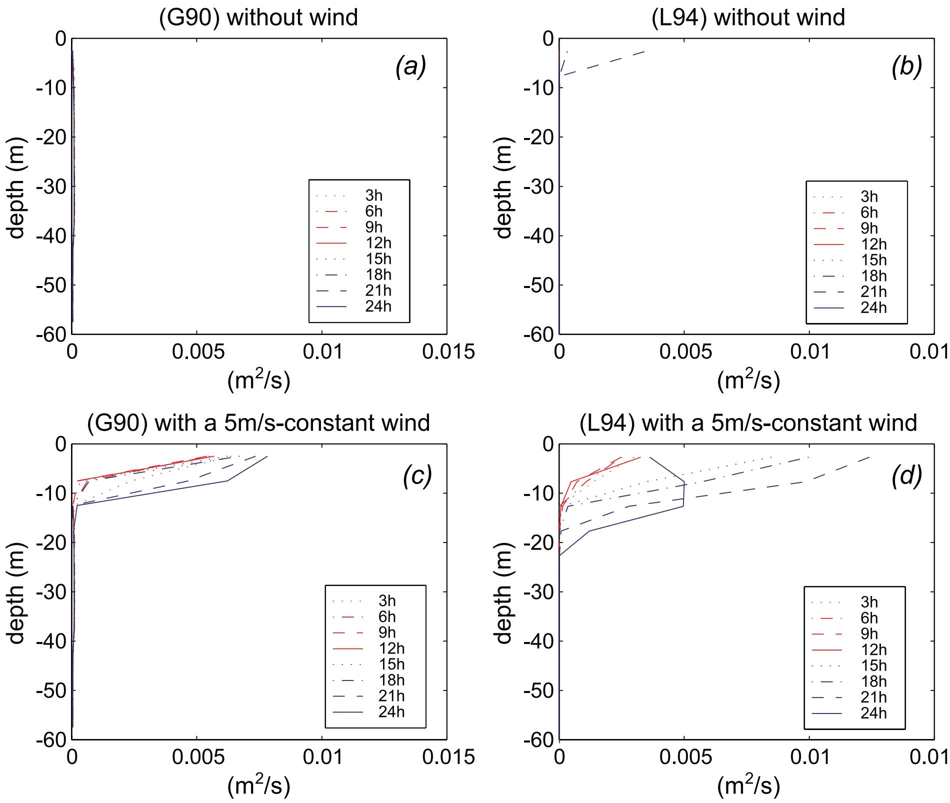

Fig. 8. Corresponding mixing coefficients at 8 h of the diurnal cycle, for day in red (3, 6, 9 and 12 h) and for night in blue (15, 18, 21 and 24 h): (a) G90 without wind, (b) L94 without wind, (c) G90 with a 5-m/s wind and (d) L94 with a 5-m/s wind. L94 results are obtained with diapycnal mixing (Eqs. (16-a,b,c)) and destabilizing term (Eq. (14)).

the other hand, L94 is able to induce such a mixing during night and limits the SST increase in the following days. We observed these features in realistic simulations over weak wind periods (period 2 in Fig. 5 for example). These tests also show the importance of diapycnal mixing (Eqs. (16-a,b,c)) in limiting the SST increase during day in L94 but also in accelerating the mixing induced by convection during night. On the other hand, the destabilizing term (Eq. (14)) has a very weak influence in these conditions.

3.3. First conclusions

The first simulations made previously in stabilizing-dominant conditions allow us to grasp several major differences between G90 an L94 parameterizations for vertical mixing. For a same wind and for the weak convection observed in Spring in the Bay of Biscay, G90 calculates very alike mixing coefficients for night and day; on the other hand, according to L94, they have a very different amplitude on night and day. Furthermore, without wind and for a weak nocturnal convection, G90 parameterization is unable to induce enough mixing to stabilize the upper layer, whereas L94 one can homogenize this layer, even without the influence of diapycnal mixing. This homogenization is due to the nonlocal character of L94 parameterization: this nonlocal character stands in the determination of the BL h by Eq. (13) and in the direct use of h in the parameterization (Eq. (12)) of the turbulent diffusion coefficient. However, the in situ data presented here do not allow us to really conclude about which of these two models is better to simulate the Spring warming of the surface layer. Under the early Spring conditions of Section 3.1.1, the effect of diapycnal mixing in L94 leads to underestimate the

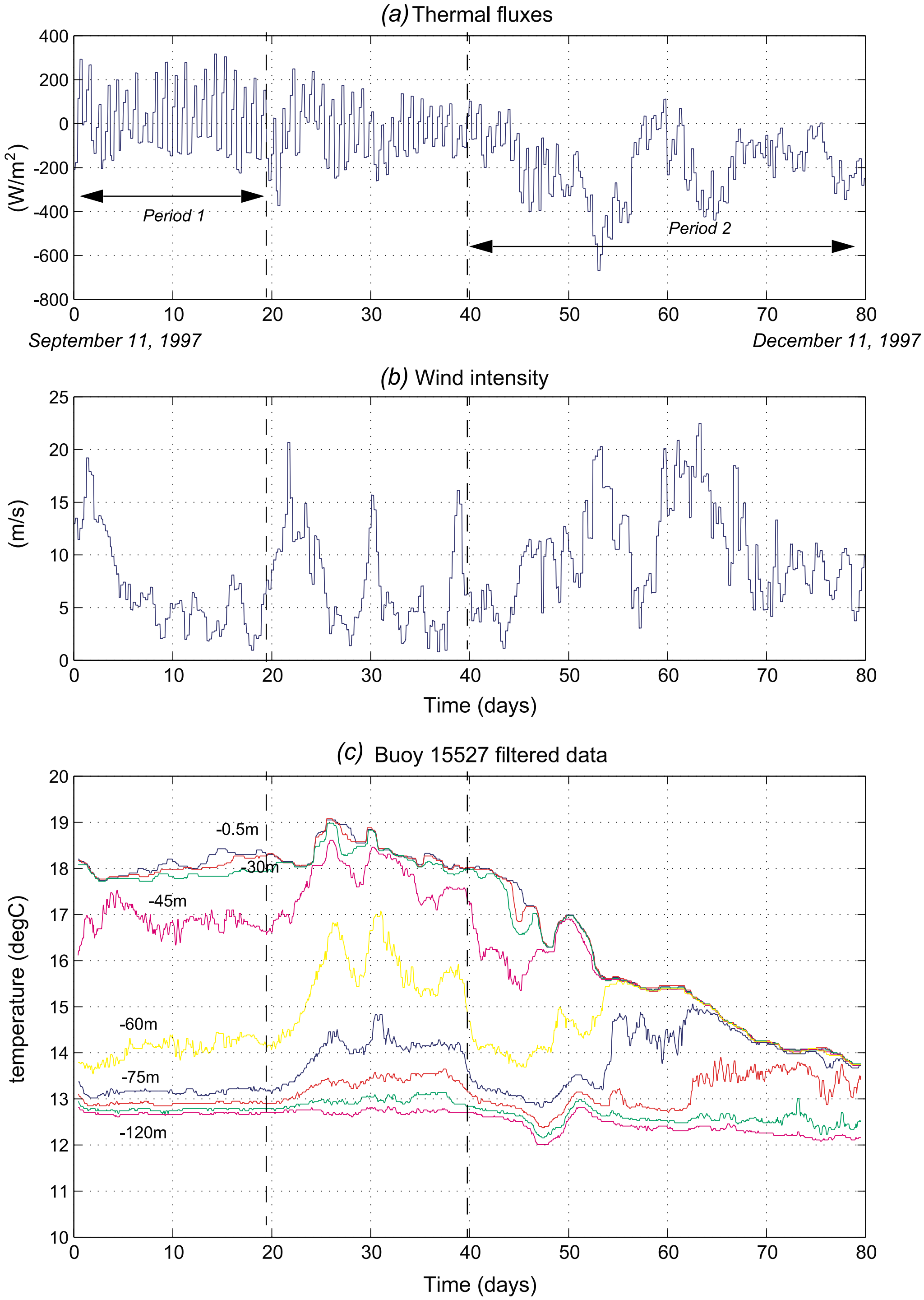

Fig. 9. Thermal fluxes (a) and wind intensity (b) issued from ARPEGE along buoy 15527 trajectory between September 11 and December 1, 1997. (c) Raw temperature evolution at thermistor depths 0.5, 15, 30, 45, 60, 75, 90, 105 and 120 m along buoy 15527 trajectory.

SST increase observed in in situ data, whereas L94 results without diapycnal mixing are in better accordance with this SST increase. However, these conclusions have to be considered with caution because advective effects are present over the second period of the simulation. Under the clearly positive thermal budget of Section 2.2.2, L94 mixing with or without diapycnal mixing is clearly too strong, whereas G90 one is too weak compared to in situ data.

4. Cases of destabilizing-dominant conditions

Let us now examine the Fall period of seasonal thermocline destruction. The limitations due to the in situ data sampling in the upper surface layer and encountered in Spring for data–models comparison are less restrictive, here, because temperature profiles present a well-formed mixed-layer of several tens of meters. We will examine results along one buoy trajectory from mid-September to mid-December. This buoy, numbered 15527, was deployed on September 11, 1997 at position (46°N–18°W). It recorded in situ data over a long period of time (9 months). Like the other ones, its trajectory was centered in the middle of the Bay of Biscay.

4.1. In situ data over the whole period

The period of interest, here, extends from September 11, 1997 to December 5, 1997: it covers the Fall mixed-layer deepening period. Wind and thermodynamical fluxes used along the buoy trajectory are issued from ARPEGE (Fig. 9a and b). After a first

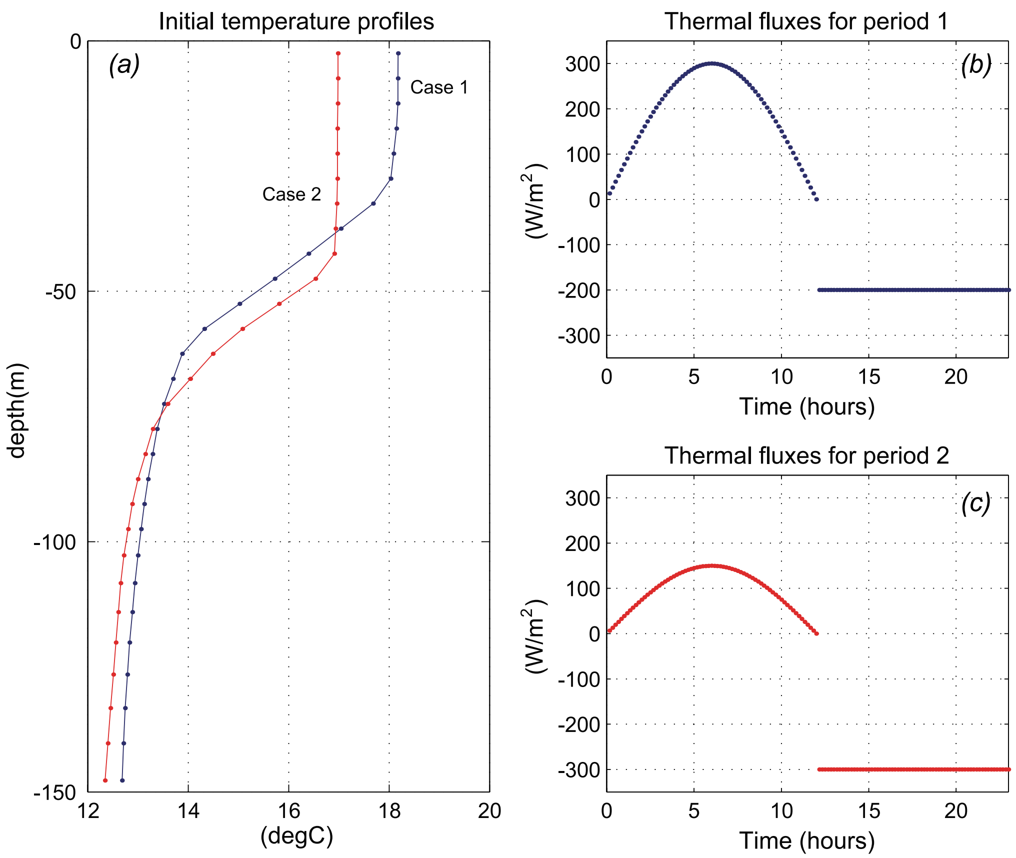

Fig. 10. Initial temperature profiles (a) and schematic thermal fluxes corresponding to periods 1 (b) and 2 (c) defined along buoy 15527 trajectory.

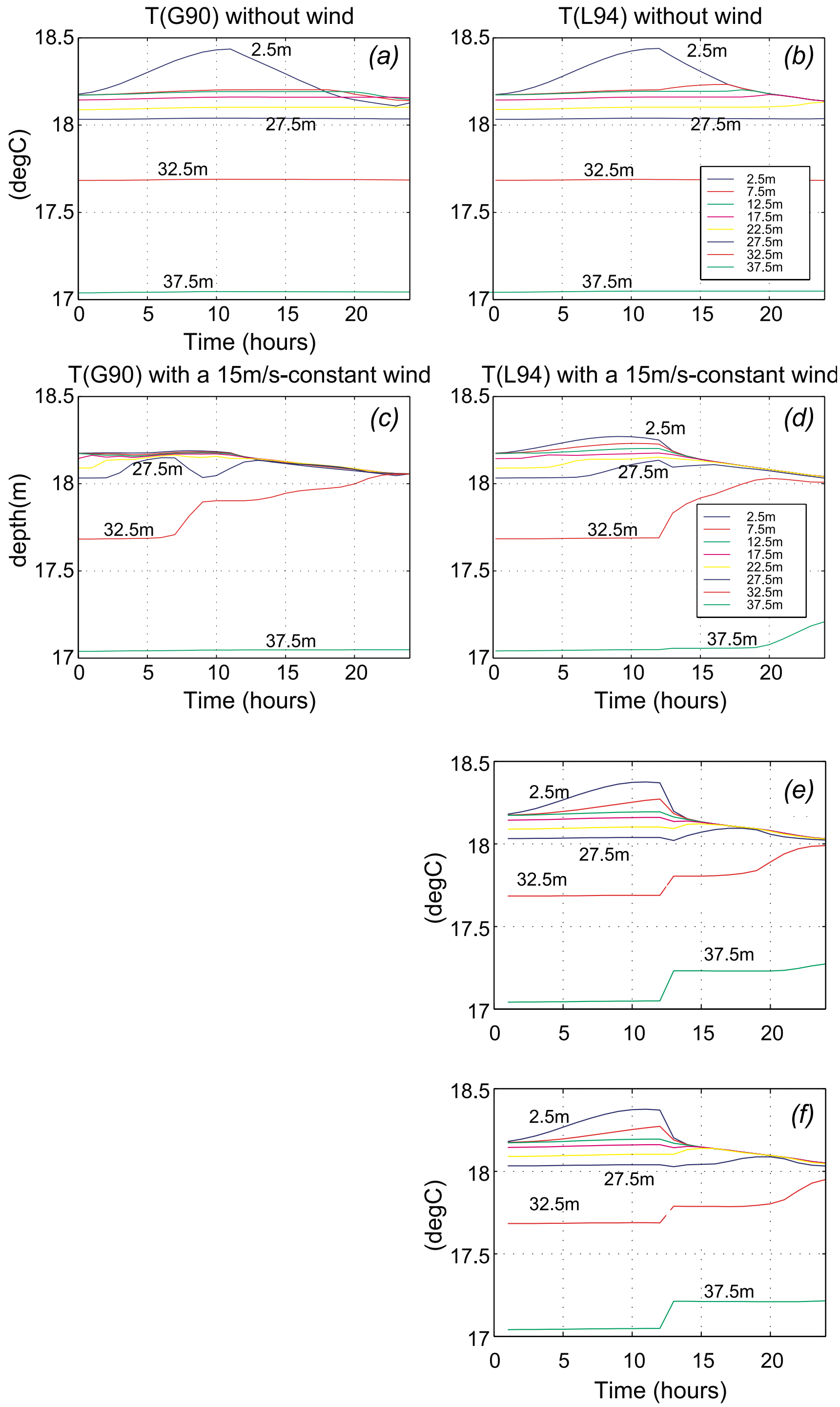

Fig. 11. Comparison of temperature evolutions over one diurnal cycle of period 1 obtained with Case 1 for initial stratification and for: (a) G90 without wind, (b) L94 without wind, (c) G90 with a 5-m/s wind, (d) L94 with a 5-m/s wind, (e) L94 with a 5-m/s wind and without diapycnal mixing and (f) L94 with a 5-m/s wind and without diapycnal mixing nor destabilizing term (Eq. (14)).

period of balanced thermal budget (days 0 to 40, i.e. from mid-September till the end of October), November is characterized by a globally negative thermal budget which speeds up the mixed-layer deepening. Between days 1 and 40, the mean wind-intensity is 5 m/s punctuated by strong wind peaks of 15 to 20 m/s. After day 40, wind is high with frequent peaks of 15 to 20 m/s.

Fig. 9c displays the 25 h-filtered in situ temperature data recorded at the different thermistor depths. Between days 20 and 40, these data highlight a phenomenon not attributable to the surface fluxes shown in Fig. 9a, but to an eddy whose signature is a global warming in the 100-m upper layer. To be consistent with the 1-D assumption of our simulations, the global period must be split into two steps before running G90 and L94 models: at first, between days 1 and 20 (period 1) and secondly between days 40 and 80 (period 2), i.e. from the initial stratification found in in situ data at day 40. Before using the realistic ARPEGE fluxes extracted along the buoy trajectory, let us examine the following schematic tests corresponding to periods 1 and 2. These schematic tests will complete those previously performed in Spring stabilizing conditions in comparing G90 and L94 parameterizations.

4.2. Schematic tests corresponding to periods 1 and 2

The schematic tests performed here are based on the mean conditions deduced from real fluxes observed on periods 1 and 2 (Fig. 9). Test 1 corresponds to period 1 and uses a sinusoidal diurnal flux with an amplitude of 300 W/m^2 and a constant night convection of -200 W/m^2 (Fig. 10b). Test 2 corresponds to period 2 and uses a sinusoidal diurnal flux with an amplitude of 150

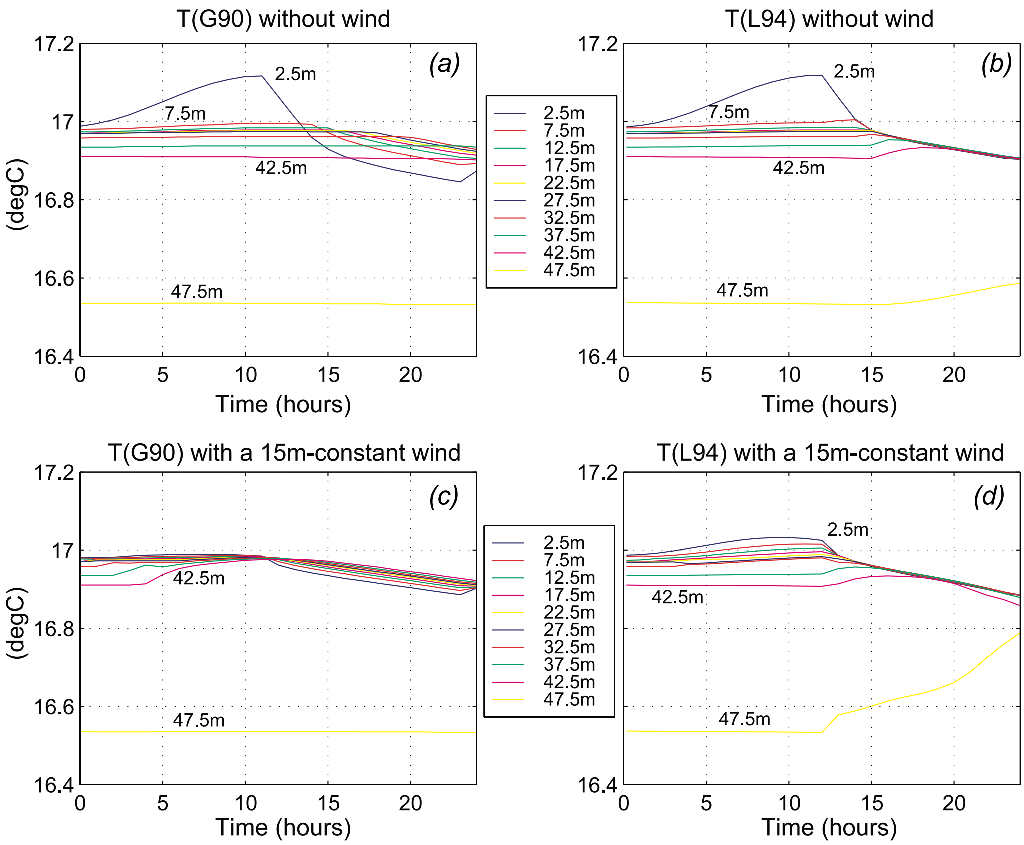

Fig. 12. Comparison of temperature evolutions over one diurnal cycle of period 2 obtained with Case 2 for initial stratification and for: (a) G90 without wind, (b) L94 without wind, (c) G90 with a 15-m/s wind and (d) L94 with a 15-m/s wind.

W/m^2 and a constant convection of -300 W/m^2 during night (Fig. 10c). Test 1 uses the initial in situ stratification denoted Case 1 for the 30-m depth mixed-layer found at day 0, whereas test 2 uses the initial stratification denoted Case 2 for the 45-m mixed-layer found at day 40 (Fig. 10a). Test 1 will examine the influence of wind intensity on a well-stated seasonal thermocline by comparing a no-wind situation with a 15-m/s constant wind one. Test 2 will examine the relative part of convection and wind in the mixed-layer deepening by comparing a no-wind situation with a 15-m/s constant wind one.

4.2.1. Test 1: influence of wind intensity on a well-stated seasonal thermocline

Fig. 11 compares G90 and L94 simulations of temperature evolution over one diurnal cycle without wind (Fig. 11a and b) and with a 15-m/s constant wind (Fig. 11c and d). For the 15-m/s wind situation, Fig. 11e and f compares the L94 results obtained without the influence of diapycnal mixing (Eqs. (16-a,b,c)) first nor destabilizing term (Eq. (14)) second.

Without wind, as in Spring results, G90 mixing is insufficient to prevent temperature inversions in the upper surface layer as shown in Fig. 11a between hours 17 and 24. As shown in Fig. 11b, L94 is able to mix the 12.5-m upper layer during night convection. This latter result is obtained even without the influence of diapycnal mixing (Eqs. (16-a,b,c)) nor destabilizing term (Eq. (14)): the results obtained with L94 without these two terms are not presented here because they lead to results similar to those shown in Fig. 11b.

With a 15-m/s constant wind, G90-calculated mixing is of the same order on day and night, whereas L94-

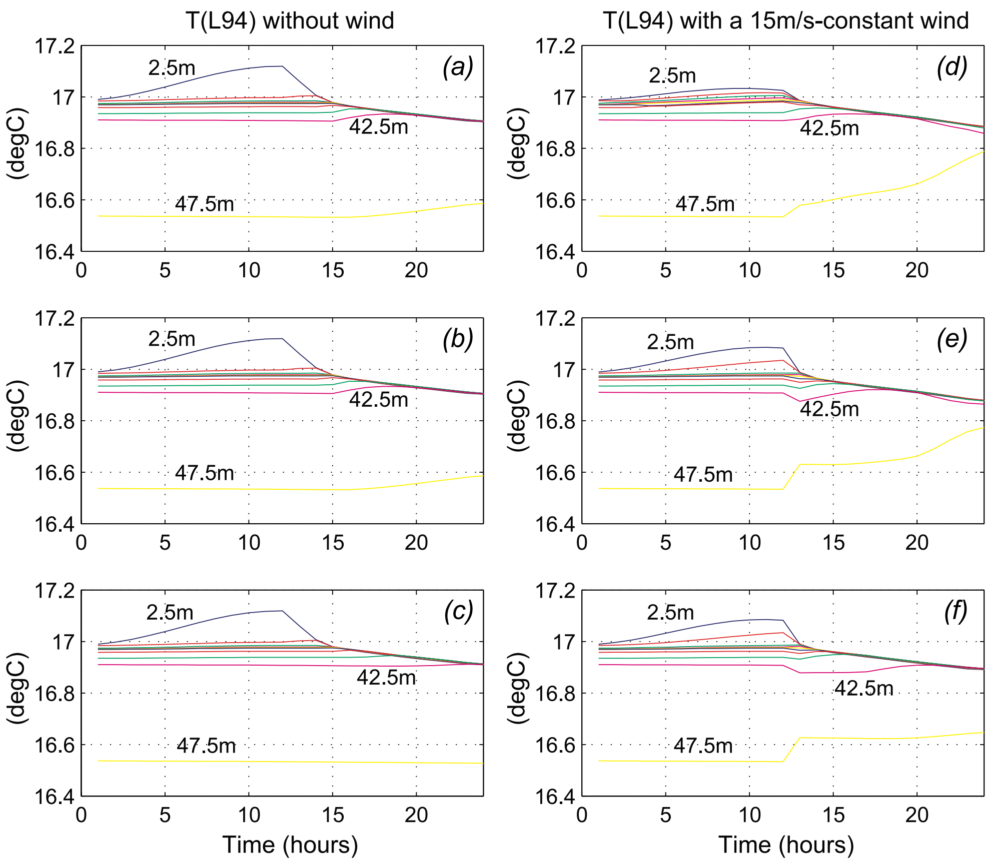

Fig. 13. Same simulations as in Fig. 12 for L94 without wind (a) without diapycnal mixing (Eqs. (16-a,b,c)) (b) nor destabilizing term (Eq. (14)) (c) and for L94 with a 15-m/s wind (d) without diapycnal mixing (e) nor destabilizing term (f).

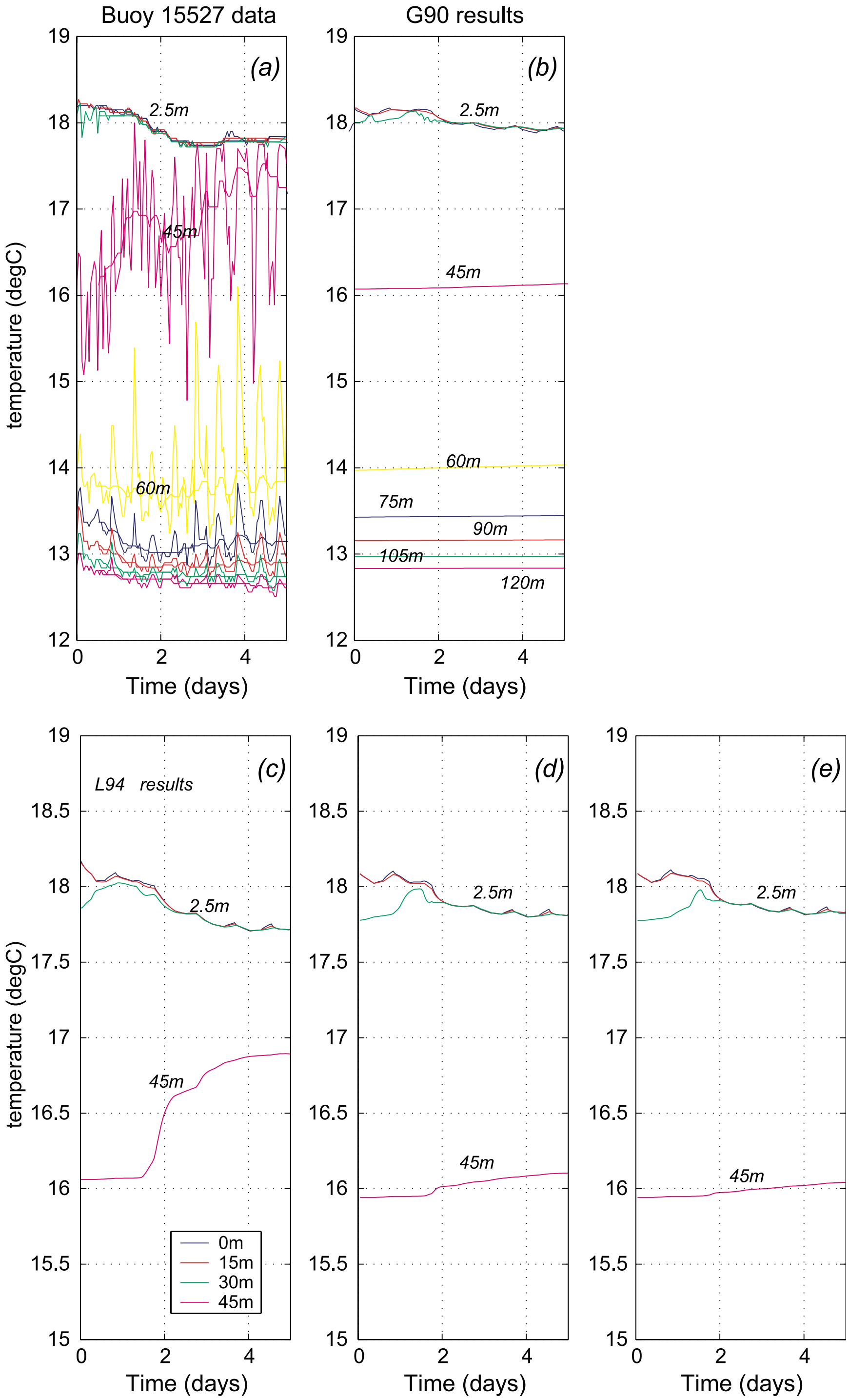

Fig. 14. Comparison of buoy 15527 in situ temperature data (a) at nine different depths with G90 (b) and L94 (c) results for the first 5 days of realistic period 1 (days 0 to 5 of Fig. 9). Figs. (d) and (e) show corresponding L94 results without diapycnal mixing (Eqs. (16-a,b,c)) nor destabilizing term (Eq. (14)), respectively.

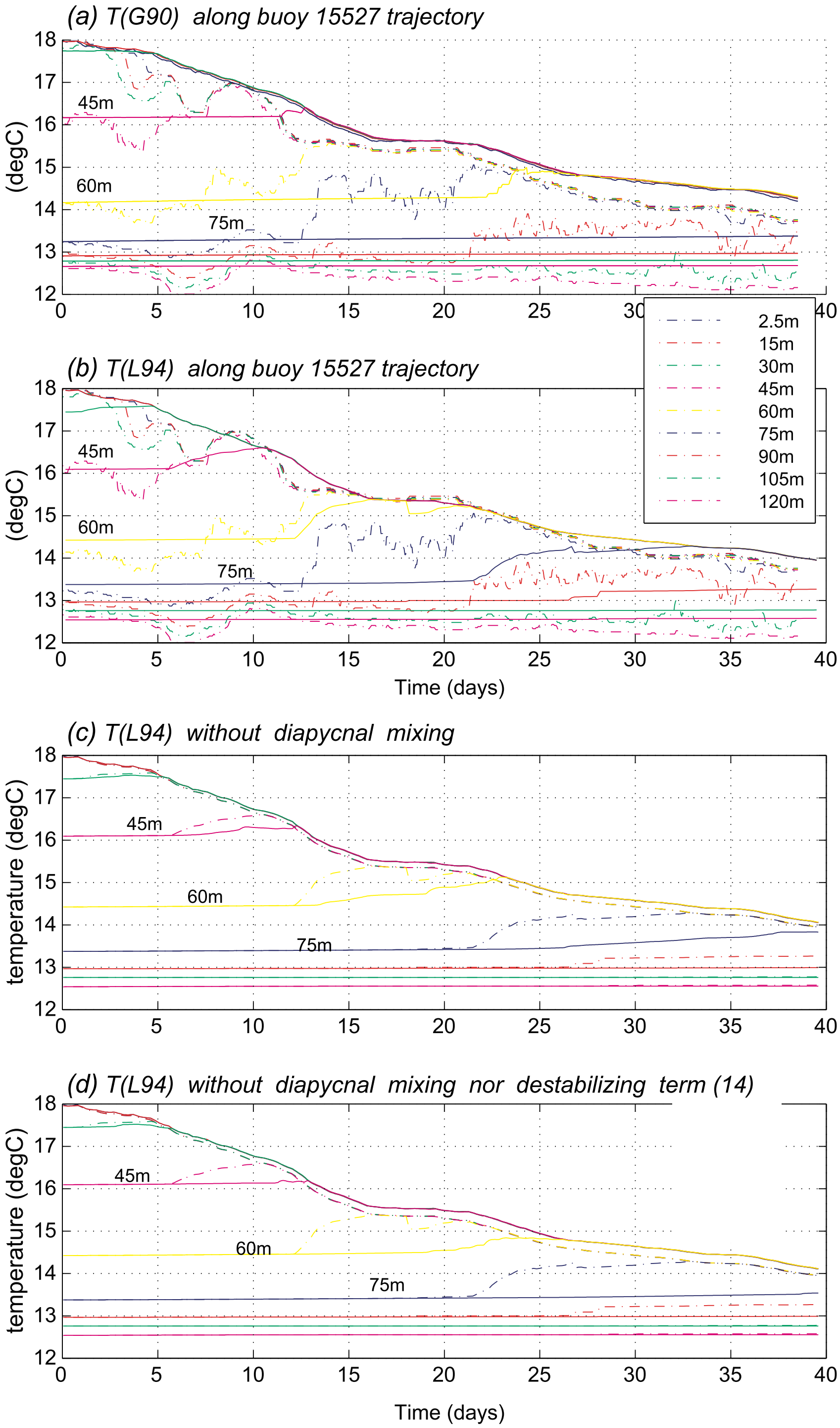
(a) T(G90) along buoy 15527 trajectory
(b) T(L94) along buoy 15527 trajectory
(c) T(L94) without diapycnal mixing
(d) T(L94) without diapycnal mixing nor destabilizing term (14)
(degC)
temperature (degC)
Time (days)
45m
60m
75m
2.5m
15m
30m
45m
60m
75m
90m
105m
120m

mixing is more contrasted. This results in a more important rise of the SST on day with L94 than with G90, whereas at night L94-calculated mixing acts down to the 37.5-m depth (Fig. 11c and d). So, the current shear induced by the 15-m/s constant wind erodes a part of the thermocline up to 32.5 m with G90 and up to 37.5 m with L94 in its complete form, whereas without wind the deepening of the mixed-layer is stopped by the thermocline stratification. By comparing Fig. 11d, e and f, we can see that this better penetration ability of L94 into the stable thermocline is mainly due to the diapycnal mixing. Without diapycnal mixing nor stabilizing term (Eq. (14)), results obtained with L94 (Fig. 11f) in term of thermocline erosion are comparable to those obtained with G90 (Fig. 11c). In this case of strong wind event with weak night convection applied on a well-stated thermocline, the diapycnal mixing is essential in eroding this stable thermocline.

4.2.2. Test 2: relative part of convection and wind in the mixed-layer deepening

Let us now examine what is the relative effect on a deep mixed-layer of either a high wind associated with a strong night convection or a strong night convection without wind. Corresponding G90 and L94 simulations are compared in Fig. 12 in terms of temperature evolution over one diurnal cycle: Fig. 12a and b shows G90 and L94 simulations without wind, whereas Fig. 12c and d show the equivalent simulations with a 15-m/s constant wind. In Fig. 13, the results obtained with L94 in its complete form are compared with those obtained with L94 without diapycnal mixing (Eqs. (16-a,b,c)) first nor destabilizing term (Eq. (14)) second: Fig. 13a, b and c shows these results without wind and Fig. 13d, e and f with a 15-m/s constant wind.

Like in the previous tests made without wind, G90 mixing is insufficient to prevent the temperature inversions in the upper layer at night (Fig. 12a). On the other hand, the mixing induced by convection only in L94 is sufficient to reach the 47.5-m depth and to cerode a part of the thermocline whose initial upper limit is located at 40 m (Fig. 12b). By comparing L94 results in its complete form (Fig. 13a) with those obtained without diapycnal mixing (Fig. 13b) nor destabilizing term (Eq. (14)) (Fig. 13c) we can see that the ability of L94 to better penetrate the mixed-layer in no-wind conditions is due to the destabilizing term (Eq. (14)): this is this term that allows the mixing to reach the 47.5-m depth. Without it, except for temperature inversions in the 42.5-m upper layer, L94 and G90 results are similar.

The night BL depth evaluated by L94 with wind is greater than the one evaluated without wind. This induces the early (from hour 13) penetration of mixing into thermoline up to the 47.5-m depth (Fig. 12d). At hour 24, the mixed-layer depth calculated by L94 reaches 47.5 m. On the other hand, under the same conditions, G90 mixing is stopped at 42.5 m by the stable thermocline. Fig. 13d, e and f shows that the effect of destabilizing term (Eq. (14)) has the same importance here than diapycnal mixing (Eqs. (16-a,b,c)) in the erosion of the thermocline up to 47.5 m. Without these two terms, L94 and G90 results are similar in term of erosion of the well-stated thermocline.

4.3. Comparison with realistic data over periods 1 and 2

Using these different results, let us now compare G90 and L94 realistic simulations over periods 1 and 2 with in situ temperature data along the buoy trajectory.

4.3.1. Period 1 with realistic fluxes from day 1 to 20

We selected here the first 5 days of period 1 (corresponding to the first 5 days of realistic fluxes shown in Fig. 9). This short period is characterized by a strong wind peak of 19 m/s at day 1. The quasi-balanced thermal fluxes used correspond to the conditions previously examined in Section 4.2.1.

Raw and 25 h-filtered data (Fig. 14a) are compared with G90 and L94 results (Fig. 14b and c,

Fig. 15. (a) Temperature evolution obtained with G90 (full line) for realistic period 2 (days 40 to 80 of Fig. 9) at nine different depths going from 2.5 to 120 m in comparison with in situ filtered data (dashed line); (b) temperature evolution obtained with L94 (full line) for the same period in comparison with in situ filtered data in dashed line; (c) results obtained with L94 without diapycnal mixing (full line) in comparison with results obtained with L94 in its complete form (dashed line); (d) results obtained with L94 without diapycnal mixing nor destabilizing term (Eq. (14)) (full line) in comparison with L94 results in its complete form (dashed line).

respectively) at the different thermistor depths. In term of mixed-layer characteristics, L94 results are clearly closer to in situ data than G90 ones. In particular, thermistor 45 m is progressively taken in the mixed-layer from the wind peak: this process is well reproduced by L94 in its complete form, whereas G90 is unable to sufficiently erode the thermocline to induce it. Fig. 14d and e compares L94 simulations without diapycnal mixing (Eqs. (16-a,b,c)) first, nor destabilizing term (Eq. (14)) second. This comparison shows that the erosion of the mixed-layer by L94 is principally due to the diapycnal mixing, whereas the destabilizing term (Eq. (14)) has a minor effect. In these conditions, L94 without diapycnal mixing, like G90, is unable to entrain the 15-m layer into the mixed-layer.

4.3.2. *Period 2 with realistic fluxes from day 40 to day 80*

The G90 and L94 models are now run from day 40 to day 80 using the initial stratification found in data at day 40 and the corresponding fluxes shown in Fig. 9. This period is characterized by strong convection and wind intensity, the conditions found in Section 4.2.2.

Fig. 15a and b compares G90 and L94 temperature evolutions at nine different depths cup to 120 m with 25 h-filtered in situ data. These figures highlight a progressive deepening of the mixed-layer from 40 m at day 0. This deepening reaches the 60-m depth at day 13 for in situ data, at day 17 with L94 and at day 25 with G90. The 75-m depth is creached at day 23 in in situ data and at day 33 with L94, whereas at the end of the simulation G90 predicts a mixed-layer depth below 75 m and even closer to 60 m. Results obtained with L94 in its complete form agree again more with in situ data than G90 ones. Fig. 15c and d compares L94 simulations without diapycnal mixing (Eqs. (16-a,b,c)) first, nor destabilizing term (Eq. (14)) second. By comparing these two latter simulations we can first conclude that term (Eq. (14)) is nearly as important as term (Eqs. (16-a,b,c)) to erode the mixed layer. This result is in agreement with schematic results found in Section 4.2.2. If we now compare Fig. 15d with Fig. 15a, i.e. the L94 results without diapycnal mixing (Eqs. (16-a,b,c)) nor destabilizing term (Eq. (14)) with G90 ones, we can see that L94 mixing without these two terms is not strong enough to erode the strong temperature gradient of the Fall thermoline. The deepening of the thermocline then reaches 60 m at day 25 only as G90.

These tests on destabilizing conditions show that L94 without diapycnal mixing (Eqs. (16-a,b,c)) nor destabilizing term (Eq. (14)) have no better ability than G90 to reproduce the mixed-layer deepening observed in Fall in the Bay of Biscay. As G90 one, the parameterization of turbulent mixing used by L94 without these two terms is unable to realistically erode the well-formed thermocline during convection and strong wind periods and, then, strongly underestimates the mixed-layer depth during Fall water cooling. On the other hand, the L94 parameterization of vertical mixing reproduces this deepening in a very satisfactory way if diapycnal mixing (Eqs. (16-a,b,c)) as well as destabilizing term (Eq. (14)) are taken into account.

5. General conclusion

The G90 and L94 models were compared on the basis of in situ data recorded along three buoy trajectories deployed in the Bay of Biscay over different periods of the year. Spring and Fall, i.e. the respective periods of formation and destruction of the seasonal thermocline, were examined in details under schematic as well as realistic conditions. Besides its basic parameterization based on the determination of the BL depth h, L94 uses the diapycnal mixing (Eqs. (16-a,b,c)) as well as the destabilizing term (Eq. (14)) acting in situations of pure convection or weak wind. We were here interested in examining influence of these two terms in improving results obtained with basic G90 and L94 parameterizations in the very different conditions found in Spring warming and Fall water cooling. These two periods have to be distinguished in term of conclusion.

First, in Spring conditions where convection is weak and acts only during night, we found that the effect of destabilizing term (Eq. (14)) is negligible. The effect of diapycnal mixing (Eqs. (16-a,b,c)) in limiting an excessive increase of SST is preponderant in results. The main difference between the basic parameterizations G90 and L94 stands in the amplitude variation of mixing coefficients between night and day: in G90 this variation is weak for it is mainly related to the wind intensity, whereas night and day relative behaviour of L94 mixing coefficient is much more contrasted under the action of sea-surface stabilizing or destabilizing conditions. Furthermore, by the nonlocal character of its parameterization contained in the determination of the BL h, L94 avoids the temperature inversions observed in G90 results during night convection. The results obtained with G90 and L94 are however debatable in Spring: G90 tends to overestimate the sea-surface warming, whereas L94 underestimates it. This is due to the night-convection treatment in each model which leads to too much mixing in the upper layer by L94 in Spring conditions of weak stratification, whereas the mixing action depth is too weak in G90 during night. In Fall conditions where the thermocline is well-stated, stratification is too strong for L94 without diapycnal mixing (Eqs. (16-a,b,c)) nor destabilizing term (Eq. (14)) to better erode this thermocline than G90. Diapycnal mixing in strong wind events and destabilizing term (Eq. (14)) in strong convection periods are then essential for L94 to realistically simulate the deepening of the mixed-layer. This study shows therefore the importance of nonlocal effects in 1D mixing models to a better representation of Fall observations.

All these simulations were performed with the 1-D assumption. So, advective effects were neglected in data: this assumption is valid under low wind conditions, but more debatable under high wind ones. Furthermore, we here neglected the mixing effect of internal tides in both models: this process will be the subject of further studies using L94 parameterization.

Acknowledgements

This study was carried out in the context of a Post-Doctoral research work in the Centre Militaire Ocanographie (CMO) of the Etablissement Principal du Service Hydrographique et Océanographique de la Marine (EPSHOM, UBrest, France). We are indebted to Dr V. Mariette and to C. Ratsivalaka for many helpful discussions on buoys data deployed during PRECOCE experiment. These data had already been the subject of an in-depth study using the Gaspar et al. (1990) model in the Bay of Biscay: it resulted in the construction of numerous tools that facilitated their use in the present study. We are grateful to Mrs. Friocourt for her assistance in the writing of this manuscript in English as well as to the reviewers for their helpful pieces of advice in improving it.

Appendix A

The full set of equations to be solved with G90 parameterization is the following one:

$$\frac{\partial U}{\partial t} - fV = -\frac{\partial}{\partial z}\left(c_k l_k e^{\frac{1}{2}} \frac{\partial U}{\partial z}\right) \qquad (A-1)$$

$$\frac{\partial V}{\partial t} + fU = -\frac{\partial}{\partial z}\left(c_k l_k e^{\frac{1}{2}} \frac{\partial V}{\partial z}\right) \qquad (A-2)$$

$$\frac{\partial T}{\partial t} = \frac{F_{\mathrm{sol}}}{\rho_0 C_P}\frac{\partial I}{\partial z} - \frac{\partial}{\partial z}\left(c_k l_k e^{\frac{1}{2}} \frac{\partial T}{\partial z}\right) \qquad (A-3)$$

$$\begin{aligned}\frac{\partial e}{\partial t} = &-\frac{\partial}{\partial z}\left(c_k l_k e^{\frac{1}{2}} \frac{\partial e}{\partial z}\right) - c_k l_k e^{\frac{1}{2}}\left(\frac{\partial}{\partial z}\overrightarrow{U}\right)^2 \\ &+ \frac{g}{\rho_0}\left(c_k l_k e^{\frac{1}{2}} \frac{\partial \rho}{\partial z}\right) - \frac{c_\varphi e^{\frac{3}{2}}}{l_\varphi}\end{aligned} \qquad (A-4)$$

These equations are solved using a matrix method based on prescription of surface and sea-bed conditions.

Appendix B

The function G found in Eq. (12) is assumed in a cubic polynomial form (Large et al., 1994):

$$G(\sigma) = a_0 + a_1\sigma + a_2\sigma^2 + a_3\sigma^3 \qquad (B-1)$$

This form allows us to match the physics peculiar to surface BL, i.e. the diffusivity (Eq. (12)), to the ocean interior one, expressed in Eqs. (16-a,b,c). Coefficients (a_0 to a_3) are determined by using both surface conditions of no turbulent transport across $d=0$ and the matching at the bottom of the BL h between Eqs. (12) and (16-a,b,c).

The turbulent velocity scale w_x found in Eq. (12) depends on stable or unstable conditions at the sea-surface. It takes the following form:

$$w_x(\sigma) = \frac{\kappa u*}{\Phi_X\left(\frac{\varepsilon h}{L}\right)} \quad \varepsilon < \sigma < 1 \quad \zeta < 0 \quad (\mathrm{B}-2-\mathrm{a})$$

$$w_x(\sigma) = \frac{\kappa u*}{\Phi_X\left(\frac{\sigma h}{L}\right)} \text{ else} \quad (\mathrm{B}-2-\mathrm{b})$$

where $u*$ is the friction velocity, κ is the von Karman constant and $\zeta = d/L$ is the stability parameter with L $(= u*/\kappa B_0)$ the Monin–Obukhov length and the sea-surface buoyancy flux, positive for stable forcing conditions and negative for unstable ones. The dimensionless profiles $\Phi_{\mathrm{x}}(\zeta)$ are issued from the similarity theory of turbulence applying in the near-surface layer $(0 < d < \varepsilon h)$. The forms used for these profiles are those defined in Appendix B of L94. Relation (B-2-a) applies in the near-surface layer for all surface conditions and in the transition zone of the BL for stable conditions. (ζ>0), whereas Eq. (B-2-b) applies only in the transition zone under unstable surface conditions.

References

Bougeault, P., Lacarrère, P., 1989. Parameterization of orography-induced turbulence in a meso-beta scale model. Monthly Weather Review 117, 1872–1890.

Gaspar, P., Gregoris, Y., Lefèvre, J.M., 1990. A simple eddy kinetic energy model for simulations of the oceanic vertical mixing: tests at station papa and long-term upper ocean study. Journal of Geophysical Research C95 (C9), 16179–16193.

Large, W.G., Mc Williams, J.C., Doney, S.C., 1994. Oceanic vertical mixing: a review and a model with a nonlocal boundary layer parameterization. Reviews of Geophysics 32, 363–403.

Mariette, V., Ratsivalaka, C., Verbèque V., Leborgne, E., 1999. CAMPAGNE PREOCOCE (PREdiction du comportement des Couches superficielles de l'Océan le long des Côtes Européennes, Tomes 1, 2 and 3, Rapport EPSHOM/CMO/RE/NP 11 du 31 mai 1999.

Mellor, G.L., Yamada, T., 1982. Development of a turbulence closure model for geophysical fluid problems. Reviews of Geophysics 20, 851–875.

Niiler, P.P., Kraus, E.B., 1977. One-dimensional models of the upper ocean. In: Kraus, E.B. (Ed.), Modelling and Prediction of the Upper Layers of the Ocean. Pergamon, New York, pp. 143–172.

Ratsivalaka, C., 1999. Dètermination du budget â l'interface air-mer: impact sur les simulations de FLORENCE, Rapport EPSHOM/CMO/RE/NP du 6 décembre 1999.